# Implementation issues and performance characterization of FDAF for a GNSS receiver

Mathieu Raimondi, Olivier Julien, Christophe Macabiau

# Implementation Issues and Performance Characterization of FDAF for a GNSS Receiver

Mathieu Raimondi, *INSA/ENAC*
Olivier Julien, *ENAC*
Christophe Macabiau, *ENAC*

## BIOGRAPHY

Mathieu RAIMONDI is a signal processing engineer. He graduated in 2005 from the ENAC (Ecole Nationale de l'Aviation Civile) in Toulouse, France. He is now a PhD Student at the ENAC and studies signal processing solutions to fight interference on GNSS receivers.

Olivier JULIEN is an assistant professor at the ENAC, Toulouse, France. His research interests are GNSS receiver design, GNSS multipath and interference mitigation and GNSS interoperability. He received his engineer degree in 2001 in digital communications from ENAC and his PhD in 2005 from the Department of Geomatics Engineering of the University of Calgary, Canada.

Christophe MACABIAU graduated as an electronics engineer in 1992 from the ENAC in Toulouse, France. since 1994, he has been working on the application of satellite navigation techniques to civil aviation. He received his Ph.D. in 1997 and has been in charge of the signal processing lab of the ENAC since 2000.

## INTRODUCTION

The future use of the Galileo E5 and GPS L5 bands by the civil aviation community raises new issues, notably concerning pulsed interference. These bands suffer concomitants radio frequency emissions from DME (Distance Measuring Equipment), TACAN (TACtical Air Navigation), JTIDS (Joint Tactical Information Distribution System) and MIDS (Multifunctional Information Distribution System) systems. These interferences, if ignored, significantly disturb GNSS receivers functioning and prevent them from meeting civil aviation requirements. In order to be used onboard civil aircrafts, the GPS L5 and Galileo E5 signals have to be processed so that they allow specified minimum performances.

In the following, the study will focus on the E5a/L5 band, as this band is more impacted by pulsed interference than the E5b one [Bastide, 2004]. Also, it can be shown that the impact of JTIDS/MIDS signals on GPS L5 and Galileo E5a signal processing is very low with respect to DME/TACAN signals' one. Consequently they will be omitted herein for simplification purposes.

The hot spot is defined as the place where the influence of DME/TACAN signals is the largest on the victim GNSS receivers. Studying the behaviour of a GNSS receiver in this particular interference environment is necessary to guarantee the receiver reaches the minimum performance specified by civil aviation authorities.

The usual Figure Of Merit (FOM) used to look at the impact of interference is the degradation of the post-correlation $C/N_0$. Indeed, it constitutes a good indicator of acquisition, tracking and data demodulation performance, which are critical operations for the receiver.

A GNSS receiver that would not use an Interference Mitigation Technique (IMT) would experience severe post-correlation $C/N_0$ degradations [Bastide, 2004]; often leading to loss of locks, in the hot spot environment.

Thus, two IMTs implemented in the RF front end were proposed. The first one is called the Temporal Blanker (TB). Its digital implementation is described in [Grabowsky, 2002], and its benefits in terms of post-correlation $C/N_0$ largely studied in [Bastide, 2004]. It shows that GNSS receivers using the technique would comply with ICAO requirements: using TB, no loss of lock is experienced and the $C/N_0$ ratio stays above the minimum requirements.

On the other hand, FDAF is proposed as an algorithm that would guarantee higher $C/N_0$ levels in presence of interference. This has already been studied through simulation results in [Raimondi, 2008], neglecting real receivers front-end effects. In addition, the post-correlation $C/N_0$ degradation was the only observed FOM, whereas some other indicators are necessary.

The paper first describes the threat of introducing new GNSS signals in an already occupied band. Then, the impact of pulsed interference, in terms of post-correlation $C/N_0$ and AGC gain disturbance will be presented. Then the FDAF algorithm is depicted, along with its capacity to remove interference. Finally, FDAF impact on post-correlation $C/N_0$, but also AGC convergence, cross-correlation functions and signal phase continuity are analysed.

## I. THREAT DESCRIPTION

The study focuses on the major threat in the L5 band: DME/TACAN ground beacons emissions. Their emissions interfere with the E5a/L5 GNSS signals, and can prevent the GNSS receivers from acquiring and tracking satellites if no care is taken. The quoted beacons

emit pulse pairs, each pulse being a Gaussian curve modulated by a cosine [Monnerat, 2003]. It can be modelled as follow:

$$s(t) = \sqrt{P} \times \sum_{k=1}^{N} \left( e^{\frac{-\alpha(t-t_k)^2}{2}} + e^{\frac{-\alpha(t-\Delta t-t_k)^2}{2}} \right) \times \cos(2\pi f_I t + \theta_I)$$

Where:

- $P$ is the DME/TACAN peak power at receiver antenna level (W),
- $\{t_k\}$ is the set of pulse pairs arrival times,
- $f_I$ is the frequency of the received DME/TACAN signal (Hz),
- $\theta_I$ is DME/TACAN signal carrier phase at the GNSS receiver antenna port,
- $\Delta t$ is the inter-pulse interval (=12µs),
- $\alpha = 4.5 \times 10^{11} s^{-2}$.

Figure 1 represents a DME/TACAN pulse pair. The ground stations emit up to 2700 (DME) / 3600 (TACAN) pulse pairs per second (ppps). The actual ppps values are proper to each station.

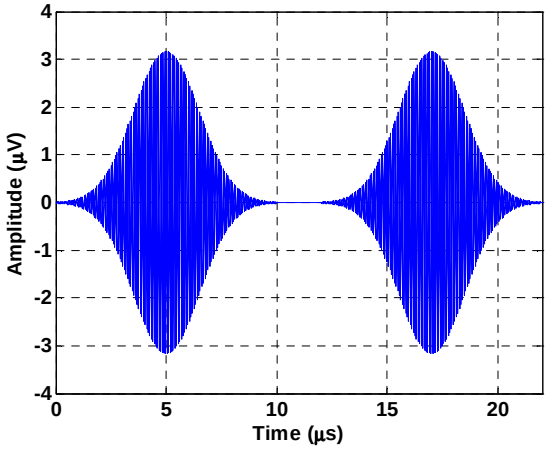


**Figure 1: DME signal pattern.**

For an onboard GNSS receiver, the operational environment is then composed of a combination of signals emitted by DME/TACAN beacons with different powers, carrier frequencies and pulse pair repetition rate.

## II. IMPACT OF PULSED INTERFERENCE ON GNSS RECEIVERS

The reception of pulsed interference by a GNSS receiver has two main effects: one on the AGC loop convergence value, the other on correlator outputs (thus on code and phase tracking).

The AGC loop is a device meant to amplify the signal so as to minimize quantization losses. Figure 2 shows the signal to noise ratio degradation as a function of the ratio between the noise standard deviation $\sigma$ and the maximum quantization level $L$. This degradation presents a minimum value, so that the AGC adapts $\sigma$ to reach this minimum value. The underlying theory can be found in [Van Dierendonck, 1996].

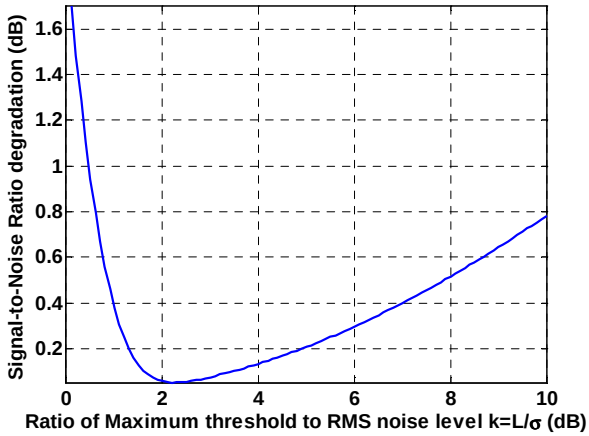


**Figure 2: SNR degradation at correlator output in presence of thermal noise only using a four bits quantizer.**

The curve was obtained assuming thermal noise only is quantized (GNSS signals are neglected). In case pulsed interference is received, the loop incorrectly estimates $\sigma$, leading to non-optimal quantization.

The suffered SNR degradation therefore depends upon the interference environment, but also the AGC gain estimation method.

Indeed, the AGC is a tracking loop, and can use different discriminators. The most natural one is the standard deviation based discriminator. Nevertheless, a discriminator based on thermal noise power estimate can be also used. This kind of discriminator is interesting as it is more robust to interference, especially when they are centred, like pulsed interference is.

In addition to increasing quantization loss, AGC gain errors imply imperfect IMTs operation. Both studied IMTs use fixed thresholds, chosen with respect to the expected noise variance at ADC output. If the AGC loop does not operate correctly, the noise variance at ADC output will be different from the one expected, thus worsening the IMTs performance.

To solve the AGC problem, the signal could be observed after the IMT is applied instead of ADC output. In this way, the observed signal can be assumed as interference free, so that the standard deviation estimation is valid.

The second effect has been extensively studied, notably in [Bastide, 2004]. After the correlation process, the received interference signals are modelled as equivalent input white noise, which density equals:

$$N_{0,I} = P_{interf} \times C_I$$

$$C_I = \int_{-\infty}^{+\infty} PSD_I \times PSD_{GNSS} df$$

Where:

- $P_{interf}$ is the interference mean power after front-end filtering,
- $C_I$ is the interference coefficient,
- $PSD_{GNSS}$ is the base-band normalized PRN code Power Spectral Density,
- $PSD_I$ is the base-band normalized interference Power Spectral Density.

The interference mean power ($P_{interf}$) is determined using an equivalent model, detailed in [Bastide, 2004] where pulses are replaced by equivalent rectangles of duration $T_{eq}$. It also uses the statistical characteristics of the signal: the interference arrives to the receiver following a Poisson law of parameter $\lambda$, which is directly linked to the PRF. It results in the following expression of $P_{interf}$:

$$P_{interf} = P \times (\lambda \times T_{eq}) \times e^{-\lambda \times T_{eq}} \times \left(1 + (\lambda \times T_{eq}) \times e^{-\lambda \times T_{eq}}\right)$$

Where:

- $T_{eq} = 2.64 \mu s$ is the equivalent duration of a pulse,
- $\lambda$ is the parameter of the Poisson law characterizing the arrival times. In our case, it equals the considered interference PRF.

The equivalent post-correlation $C/N_0$ is then:

$$\frac{C}{N_{0\ equ}} = \frac{C}{N_0 + N_{0,I}}$$

Where:

- $C$ is the carrier power,
- $N_0$ is the thermal noise density,
- $N_{0,I}$ is the equivalent noise density induced by interference.

This $C/N_0$ degradation can be mitigated by removing interference, using an IMT. The function of the IMT is to remove as much interference energy as possible, while removing as less PRN code energy as possible.

However, the suffered degradations depend upon the AGC gain estimation method, the interference environment, and the used IMT. Two IMTs are described in subsequent sections.

## III. TEMPORAL BLANKER DESCRIPTION

The temporal blanker, referred as digital pulse blanking in [Grabowsky, 2002], was the first technique proposed to mitigate pulsed interference effects on GNSS receivers. The temporal blanker detects pulsed interference by observing the input signal amplitude after the ADC (Analog to Digital Converter), and replaces the corrupted samples by zeroes. In [Bastide, 2004], the following post-correlation $C/N_0$ degradation theoretical derivation is proposed:

$$\deg\left(\frac{C}{N_{0\ equ}}\right) = \frac{1 - Bdc}{1 + \frac{\sum_i P_{jammer,i} \cdot C_I(\Delta f_i)}{\beta N_0}}$$

Where:

- $Bdc$ is the Blanker duty cycle, percentage of time the Blanker is 'active' (a sample is zeroed).
- $\beta$ is the thermal noise power reduction at correlator output due to front-end filtering.

## IV. FDAF DESCRIPTION

The FDAF technique is a pulsed interference removal technique working in the frequency domain. It was first proposed as a DME/TACAN mitigation technique in [Monnerat, 2003]. The technique intervenes in the same place as the temporal blanker; the input of the algorithm is therefore a quantized and sampled signal. It performs an estimation of the incoming signal's Fourier transform, by operating a Fast Fourier Transform (FFT) on a pre-defined number of samples ($R$). It then compares the magnitude of each point of the signal's Fourier representation to a certain threshold. Note that since the incoming signal is, without disturbances, dominated by thermal noise, the FFT representation of the incoming signal should ideally be flat (white). This assumption allows the determination of a threshold that would represent the usual noise level, with a certain false alarm rate. If certain points of the incoming signal's Fourier transform exceed this threshold, they are considered corrupted by an interference and set to zero. Finally, the inverse FFT of the manipulated incoming signal is performed so as to obtain the signal back in the time domain to feed the acquisition/tracking modules.

The relative narrow frequency representation of DME/TACAN signals (~1 MHz, see Figure 3) compared to the E5a/L5 GPS and Galileo signals (~20 MHz wide) allows this targeted blanking.

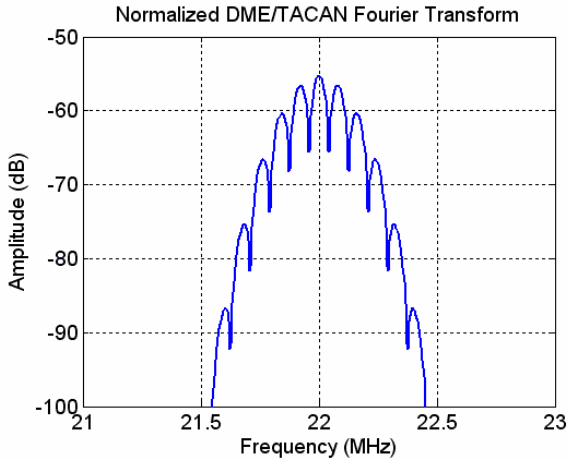


**Figure 3: DME/TACAN Signal Normalized Fourier Transform modulated at 22 MHz.**

In order not to be a computation burden, the Fourier analysis requires the incoming signal to be split into pieces composed of a relatively small pre-determined number of samples. A large number of samples would increase the frequency resolution of the Fourier transform and would likely result into a more relevant blanking technique. However, it will also induce an increase in the computation load (FFT of an increased number of points). A trade-off between performance and computation load has then to be found. In the following tests, this value is set to 128, as [Raimondi, 2006] stated this setting showed good performance and reasonable additional complexity. Indeed, using a sampling frequency of 56 MHz, each window is 2.28 µs long, which corresponds to half the duration of a pulse.

Figure 4 details the functioning of the technique. An example of a piece of signal corrupted by a DME signal is passed through the FDAF.

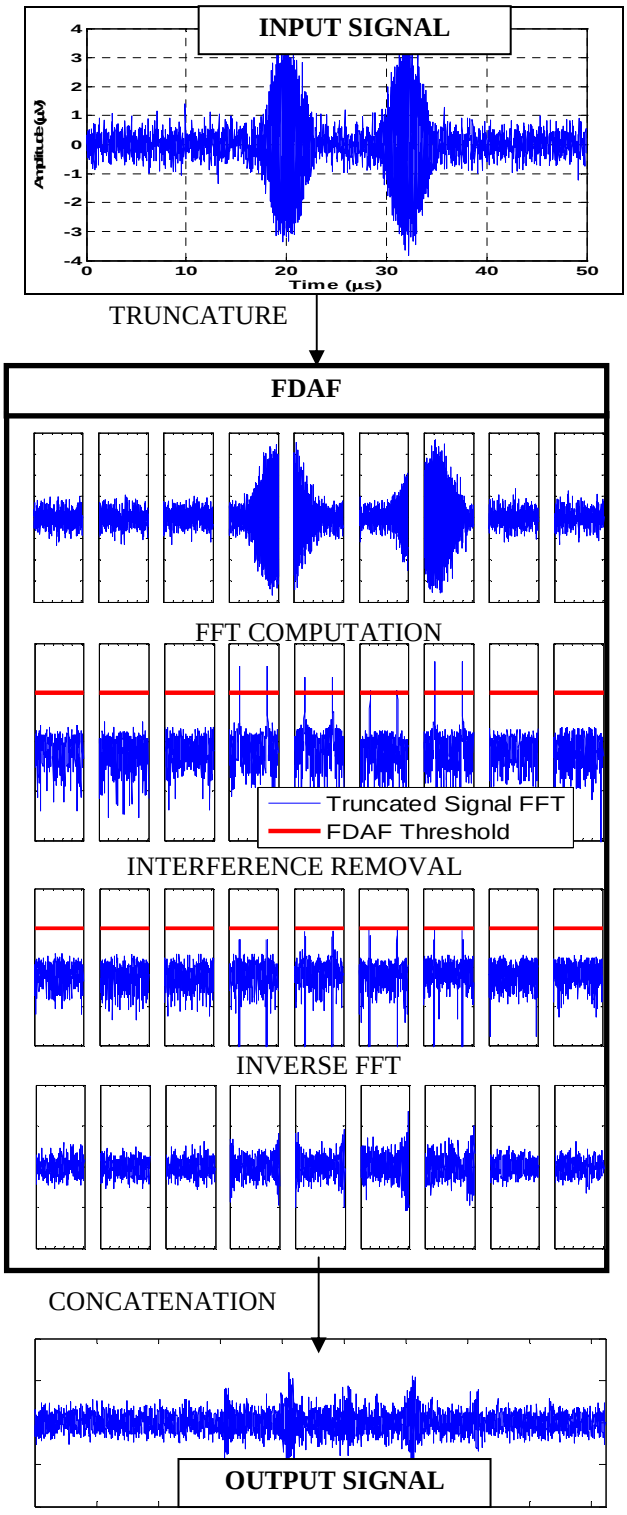


**Figure 4: FDAF Functioning Scheme.**

The robustness of a GNSS receiver to pulsed interference can be improved using an IMT.

## V. PERFORMANCE ANALYSIS METHODOLOGY

Processing a GNSS receiver signal using TB or FDAF helps removing pulsed interference, but also distorts the useful GNSS signal. As said in the introduction, the major FOM is the $C/N_0$, but it is not sufficient to assess

the performance of the receiver: the impact of such processing on cross correlations is not addressed by $C/N_0$ analyses, as well as the fact that such abrupt processing (zeroes introduced in the signal) can create discontinuities in code and carrier phase measurements.

These FOMs greatly affect GNSS receivers performance: code and carrier phase for obvious reasons, and PRN isolation also, as worsening it leads to an increase of false acquisitions, and so of the mean acquisition time.

## VI. SIMULATION SETUP

The performances of the techniques were obtained using a software simulator called PULSAR, depicted in [Bastide, 2004]. The simulator is developed under Labview and is composed of:

- A signal generation block. This block generates an E5a signal, thermal noise, and pulsed interferences,
- A signal processing block composed of a front end filter, an AGC/ADC, the two presented IMTs and correlators,
- Code and carrier phase tracking loops.

Then, a $C/N_0$ estimator provides its value at correlation output. The carrier to noise density is estimated using the following formula [Betz, 2000]:

$$\frac{C}{N_0} = \frac{E[I_P]^2}{Var[I_P]} \times B_{PD}$$

Where:

- $I_P$ are the prompt Inphase samples,
- $B_{PD}$ is the PreDetection Bandwidth.

The number of inphase samples used in the mean and the variance estimators was set to 10. The predetection bandwidth is the inverse of the coherent integration time, which is the time required to output one correlator sample (10 ms in our case). Then, each carrier to noise density ratio estimate is passed through an averaging filter using 4 values.

## VII. SIGNAL ENVIRONMENT ASSUMPTIONS

The GNSS signal is a QPSK modulated L5 code, which reception power equals -155 dBW. Only the pilot channel is generated (absence of navigation data), as tracking performance only are observed. The signal, modulated at IF (14 MHz), can be written as follows:

$$s_{GNSS}(t) = \sqrt{P} \times c_{L5}(t-\tau) \times \cos(2\pi f_{IF}(t-\tau) + \theta)$$

Where:

- $P$ is the GNSS signal power at front end input,
- $c_{L5}(t-\tau)$ is the L5 code delayed by the transmission time between the satellite and the receiver $\tau$,
- $f_{IF}$ is the intermediate frequency.

The noise is white and Gaussian, and its density equals -200 dBW/Hz. The pulsed interferences follow the theoretical expression given in section I. The visible interferences are determined using the radio electric horizon, and the DME/TACAN signals reception is assumed to follow a Poisson law. Their peak power at receiver front end level is supposed to be attenuated by the DME/TACAN station antenna (see Figure 5), propagation, and the aircraft antenna (see Figure 6). More precisely, interference signals were generated assuming the GNSS receiver was located over the European hot spot. From a database composed of DME/TACAN beacon coordinates, emission powers, carrier frequencies and PRF, it calculates the link budget and outputs a file readable by the simulator gathering the required information. Then, a Matlab routine generates the interfering signal combining the DME sources received by the receiver at arrival times determined using a Poisson law.

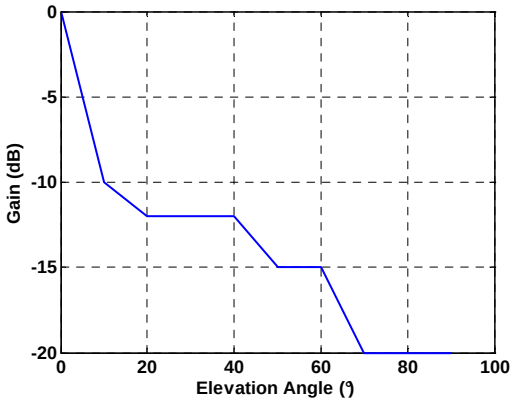


**Figure 5: DME/TACAN antenna gain pattern.**

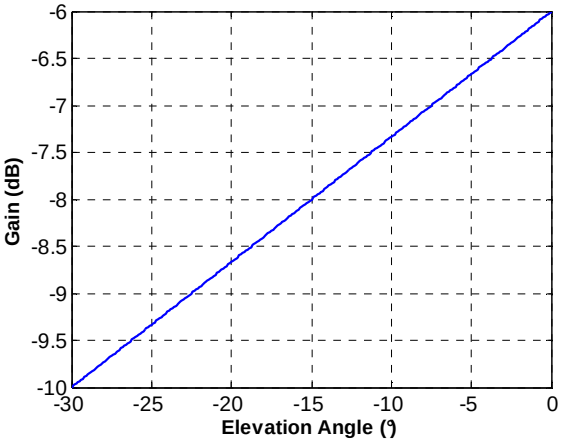


**Figure 6: GNSS aircraft antenna gain pattern.**

The total signal, thus composed of the GNSS signal, thermal noise and pulsed interference, is filtered by a FIR which order equals 50. This filter copes with the EUROCAE RF mask defined for E5a, as shown in Figure 7.

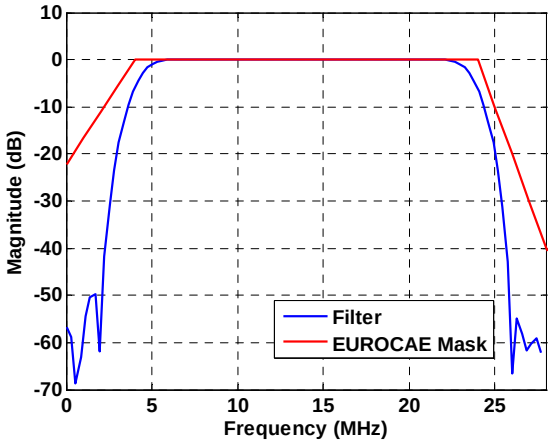


**Figure 7: Simulator FIR Transfer Function Magnitude.**

## VIII. AGC-ADC IMPLEMENTATION

As stated in section II, both quantization and IMTs performance are affected by the AGC loop behaviour. Thus, the AGC implementation requires special care, as its robustness to interference is directly involved in the receiver's performance. In a GNSS receiver, the AGC loop is implemented as shown in Figure 8.


**Figure 8: AGC Implementation.**

The quantized signal is used to estimate the gain to apply at AGC level. In the present study, the loop error voltage is implemented as follows:

$$\varepsilon = 2 \times N_0 - N_1 - N_{-1}$$

Where:

- $N_0$ is a variable incremented each time a zero comes out the ADC,
- $N_1$ is a variable incremented each time a one comes out the ADC,
- $N_{-1}$ is a variable incremented each time a minus one comes out the ADC.

This estimator is based on the ADC output signal distribution. This signal being supposed Gaussian, the estimator values only depends upon ADC quantization levels and signal variance. The estimator is therefore a function of the variance, which is a function of the gain.

The variables ($N_0$, $N_1$, $N_{-1}$) are reset to zero every 1 ms (5600 samples). Figure 9 shows there is a bijection between ε and the signal power.

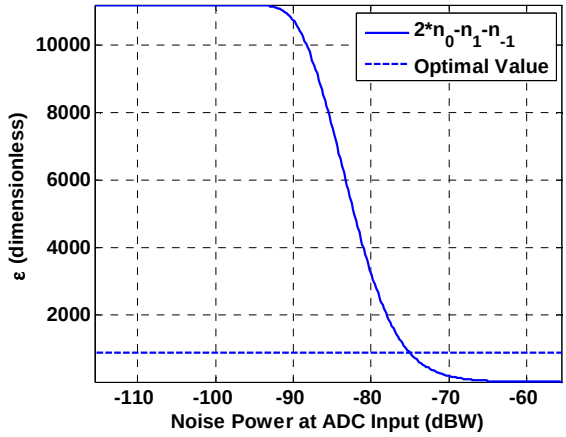


**Figure 9: Distribution Estimator Law.**

The presence of interference will modify the estimator behaviour, resulting in an error on the AGC gain, thus on the ratio k presented in section II. It induces a quantization loss increase, as shown in Figure 2.

The AGC gain error also impacts the IMTs operation. The IMTs thresholds are set to optimize IMTs performance, with respect to a given noise floor. When pulsed interference is received the AGC gain is underestimated. At IMTs input, the noise floor is therefore lower than expected, and the IMTs thresholds are not adapted anymore.

The ADC implementation is also decisive, as it can be a source of signal distortions. The IMTs were designed to detect and remove pulsed interference. ADC saturation would then severely modify the interference properties, and so the IMTs efficiency.

It requires the implementation of an ADC disposing of 8 bits, while only 4 are effectively used by acquisition/tracking modules. The 4 remaining bits are used to avoid interference distortion, this is called the dynamic range, as shown in Figure 10.

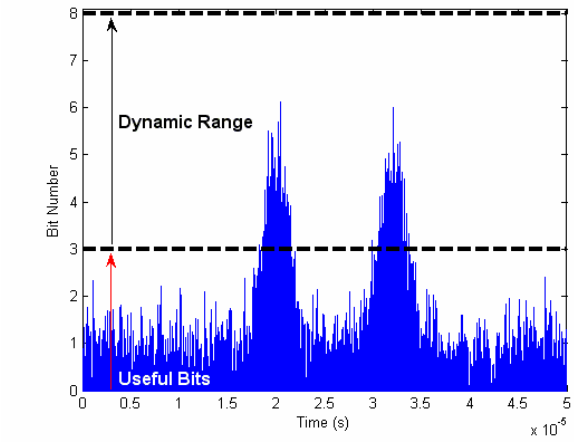


**Figure 10: AGC/ADC implementation.**

## IX. IMTs SETTINGS

The Temporal Blanker threshold has been set to -117.3 dBW, which is considered as the threshold minimizing

$C/N_0$ degradations on E5a due to pulsed interference over the European hot spot [Bastide, 2004]. The FDAF window size has been set to 128 samples, and the threshold to -195 dBW/Hz, optimizing FDAF performance over the European hot spot. In addition, the FDAF is always active, even when interference are not received. The signal being noisy, some false alarms can occur, therefore inducing $C/N_0$ loss. Using this threshold, this loss does not exceed 0.5 dB.

The threshold values are defined w.r.t. the specified noise density. In [Bastide, 2004] tests, the TB shows optimal performance using a threshold value equivalent to -117.1 dBW, assuming a noise floor of -200 dBW/Hz. Implementing the technique means digitizing this threshold, using the following formula:

$$Th_{\text{analog}} = 20 \times \log_{10}\left(\frac{Th_{digital} - 1}{G}\right)$$

Where:

- $Th_{digital}$ is the TB threshold implemented in the simulator,
- $G$ is the gain applied to the signal between front end and TB input,
- $Th_{\text{analog}}$ is the threshold in dBW.

The FDAF threshold can be expressed in dBW/Hz, in the spectral domain. The formula linking the implementation to the theoretical value is:

$$Th_{ana\log} = 10 \times \log_{10}\left(Th_{digital} \times \frac{T_s}{R} \times \frac{1}{G^2}\right)$$

Where:

- $Th_{ana\log}$ is the threshold expressed at RF input, in dBW/Hz,
- $Th_{digital}$ is the threshold to be implemented in the receiver/simulator,
- $T_s$ is the sampling period, in seconds,
- $R$ is the number of samples used in the FFT calculation.

## X. IMTs EFFECTS ON TRACKING GNSS SIGNALS: $C/N_0$ IMPROVEMENTS

Four scenarios were tested: the two IMTs are tested first using a constant AGC (optimal), then using a regulated one (as detailed in section VIII).

The performance in the four tests is given in Table 1. In case the AGC gain value is fixed, it has been set to 21.2 dB. This gain is the one minimizing quantization loss, in the simulations conditions, assuming thermal noise only is received. Figure 11 shows the AGC gain values as a function of time, using the AGC-ADC implementation described in section VIII. The presence of interference induces a bias of approximately 1 dB in the AGC gain estimation. Referring to Figure 2, this bias does not engender significant SNR degradations. In addition, the AGC gain standard deviation is lower than a $10^{th}$ of dB. Therefore, the error on the AGC gain should not exceed 1.5 dB, which is, still according to Figure 2, negligible in terms of additional quantization loss.

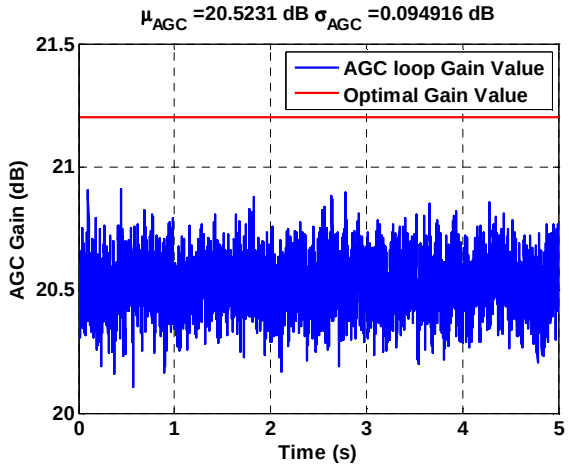


**Figure 11: AGC Loop Values**

As said in section II, AGC gain biases can also affect the IMTs performance. Table 1 compares the performance of both IMTs, activating or not the AGC loop. The $C/N_0$ degradation due to imperfections in the proposed AGC is smaller than 0.5 dB for both IMTs. If a traditional AGC had been used, the degradation would have been much larger.

In addition, these results well show the performance improvement brought by the FDAF. The gain is of about 7 dBs over the hot spot, which may justify the implementation of the technique.

**Table 1: AGC Impact on IMTs Performance**

| | $C/N_0$ Degradation (dB) | |
|---|---|---|
| **IMT** | **Fixed AGC** | **Proposed AGC** |
| **TB** | 9.2 | 9.9 |
| **FDAF** | 2.7 | 2.9 |

It is possible to use even more samples in the Fourier Transform estimation (256, 512…) but the corresponding performance increase may not be significant enough.

These $C/N_0$ degradations, obtained in "worst case" scenarios, allow an airborne GNSS receiver complying with ICAO requirements, using either IMT. Nevertheless, the 7 dB improvement due to FDAF allow loosening implementation constraints on the rest of the receiver. Indeed, the acquisition/tracking loops architecture is meant to operate in low $C/N_0$ conditions, which is increased in case TB is replaced by FDAF.

## XI. IMTs EFFECTS ON TRACKING GNSS SIGNALS: CODE AND PHASE MEASUREMENTS

[Van Dierendonck, 1996] stated that interference can be equivalently modelled as additive white noise, because of the correlation process. Thus, receiving pulsed

interference should result in an increase of both code and phase measurements standard deviations.

Nevertheless, the IMTs implemented introduce abrupt changes in the signal, which can be a source of discontinuities. This has to be carefully monitored, as these discontinuities can create unexpected effects on code and carrier phase measurements.

Concerning FDAF, this can be theoretically modelled. Indeed, the FDAF is a kind of filter, defined by block of *R* samples, which transfer function is defined in the Fourier domain:

$$S_{FDAF}(k,f) = S(k,f) \times FDAF(k,f)$$

Where:

- $k$ is the block number,
- $f$ is the frequency
- $S(k,f)$ is the input signal k[th] block FFT,
- $S_{FDAF}(k,f)$ is the FDAF output signal k[th] block FFT,
- $FDAF(k,f)$ is the kth FDAF transfer function.

In time domain, assuming one specific block (k=1), one can write:

$$\begin{aligned} s_{FDAF}(n) &= FFT^{-1}(S_{FDAF}) \\ &= \frac{1}{R}\sum_{l=0}^{R-1} FDAF(l)S(l)e^{j\frac{2\pi}{R}nl} \end{aligned}$$

Considering FDAF as a transfer function, it can be written as a function of its impulse response:

$$FDAF(l) = \sum_{n=0}^{R-1} h(n)e^{-j\frac{2\pi}{R}nl}$$

Then,

$$\begin{aligned} s_{FDAF}(n) &= \frac{1}{R}\sum_{l=0}^{R-1}\left(\sum_{n_1=0}^{R-1} h(n_1)e^{-j\frac{2\pi}{R}n_1 l}\right)\times \\ &\quad \left(\sum_{n_2=0}^{R-1} x(n_2)e^{-j\frac{2\pi}{R}n_2 l}\right)e^{j\frac{2\pi}{R}nk} \\ &= \frac{1}{R}\sum_{n_1=0}^{R-1}\sum_{n_2=0}^{R-1} x(n_2)h(n_1)\sum_{l=0}^{R-1} e^{-j\frac{2\pi}{R}(n_1+n_2-n)l} \\ &= \sum_{n_1=0}^{R-1}\sum_{n_2=0}^{R-1} x(n_2)h(n_1)\delta^{i\cdot R}_{n_1+n_2-n} \\ &= \sum_{n_1=0}^{R-1} h(n_1)x\left((n-n_1)_{\mathrm{mod}\, uloR}\right) \end{aligned}$$

$$\begin{aligned} &= \sum_{n_1=0}^{R-1} h(n_1)x(n-n_1) + \sum_{n_1=0}^{R-1} h(n_1)x(n-n_1+R) \\ &= \sum_{n_1=0}^{N-1} h(n_1)x(n-n_1) + \sum_{n_1=-N}^{-1} h(n_1+R)x(n-n_1) \\ s_{FDAF}(n) &= \sum_{n_1=-R}^{R-1}\left(h(n_1)+h(n_1+R)\right)\cdot s(n-n_1) \\ &= \sum_{n_1=-R}^{R-1} h'(n_1)\cdot s(n-n_1) \end{aligned}$$

The FDAF output signal is then the output of a filter which impulse response equals *h'*. Now, looking for symmetry in the impulse response, one can write:

$$\begin{aligned} h'(n) &= h(n) + h(n+N) \\ &= h(n) \qquad if\ n \geq 0 \\ &= h(n+N) \qquad if\ n < 0 \end{aligned}$$

And

$$\begin{aligned} h'(-n) &= h(-n) + h(-n+N) \\ &= h(-n+N) \qquad if\ n \geq 0 \\ &= h(-n) \qquad if\ n < 0 \end{aligned}$$

In case n<0, making n'=-n

$$\begin{aligned} h'(n) &= h'(-n') = h(N-n') \\ h'(-n) &= h'(n') = h(n') \end{aligned}$$

As FDAF is real, h is symmetric. So, one can write:

$$h'(n) = h'(-n)$$

On each block, FDAF operates a filtering process, which impulse response is even. Thus, each block is processed by a zero phase filter. Therefore, theoretically, FDAF should not modify the signal phase, and no discontinuities should be observed. Simulations were run to check this theoretical result. Code and carrier phase measurements were observed, and their standard deviation calculated and compared to theory. Tracking the pilot channel, [Van Dierendonck, 1996] shows:

$$\sigma^2_{PLL} = \frac{2B_{PLL}}{\frac{C}{N_0}}\left(rad^2\right)$$

$$\sigma^2_{DLL} = \frac{B_{DLL}d}{\frac{C}{N_0}}\left(chip^2\right)$$

Where:

- $B_{PLL}$ is the PLL equivalent loop noise bandwidth (Hz),
- $\frac{C}{N_0}$ is the received GNSS signal carrier to noise density ratio,
- $B_{DLL}$ is the DLL equivalent loop noise bandwidth (Hz),
- $d$ is the early/late delay (chip).

The comparison is made in Table 2. During these simulations, the AGC was disabled, and it lasted 5 seconds. The code and carrier phase measurements is in accordance with theory, whatever the IMT used. Using TB, the average estimated $C/N_0$ equalled 35.1 dB.Hz, and 42.1 dB.Hz using FDAF.

**Table 2: Simulation vs. Theoretical code and carrier phase measurements standard deviation**

| | Measured / Theory | |
|---|---|---|
| **IMT** | $\sigma_{DLL\ (cm)}$ | $\sigma_{PLL\ (cm)}$ |
| **TB** | 54.8/58.2 | 0.36/0.21 |
| **FDAF** | 26.4/27.2 | 0.165/0.10 |

## XII. IMTs EFFECTS ON PRN ISOLATION

PRN codes used in GNSS are chosen, amongst other criteria, for the isolation between cross correlation and auto correlation peaks. This isolation allows reducing false acquisition, hence improving the mean acquisition time.

If IMTs modify the isolation between these functions, it will also impact the mean acquisition time. It is though tremendous to carefully monitor this possibility. In the following, the IMT impact on PRN isolation is conducted assuming no Doppler offset.

In [Bastide, 2004], the effect of TB on the autocorrelation peak is derived from the Bdc:

$$R_{C,TB}(\tau) = (1 - Bdc) \times R_c(\tau)$$

Where:

- $R_{C,TB}(\tau)$ is the autocorrelation function when the received signal is processed by TB,
- $Bdc$ is the Blanker duty cycle, percentage of time the TB is active, i.e. the signal is replaced by zero.
- $R_C(\tau)$ is the autocorrelation function when the received signal is not processed by TB.

Then, the cross-correlation function is calculated simulating the TB effect. The GPS L5 codes of PRNs 1 to 37 were generated using Matlab.

Then, the effect of TB was simulated by zeroing some of the code chips. The number of chips to zero was determined using the Bdc value obtained by simulations in sections X and XI, where it equalled 35%. The zeroing instants are randomly determined, as the interference reception instants, and so the blanking instants, are random.

The cross-correlation function of two PRNs is then calculated. PRN 1 is chosen as the local code, the others are thus the received and TB processed ones. The maximum value of this cross-correlation is then stored. This process is repeated 1000 times, and the average maximum is calculated. The isolation is then calculated by dividing the autocorrelation peak value presented above by the presently calculated average maximum cross-correlation peak.

Figure 12 shows the simulation results. In average, the isolation is decreased by 2.2 dBs, with a maximum degradation of 3 dBs.

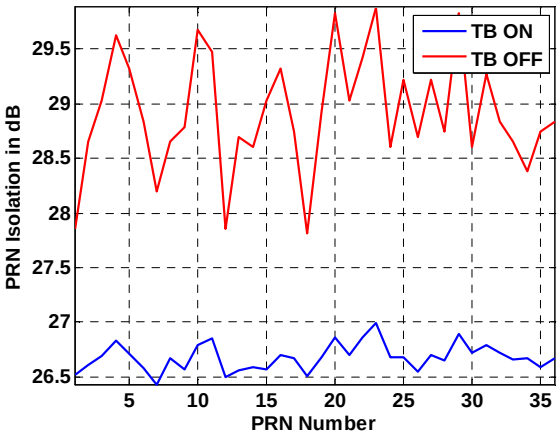


**Figure 12: TB impact on PRN isolation between PRN 1 and the rest of the constellation.**

The effect of FDAF on PRN isolation is derived using more complicated simulations. The input signal is composed of a GPS L5 signal, thermal noise and pulsed interference, both generated as described in section VII. The total signal is also filtered by the FIR described in the same section, and is then processed by FDAF, which threshold is set to -195 dBW/Hz. Then, the GPS signal is isolated and processed by the same FDAF. Finally, it is demodulated and correlated during 1 ms with the locally generated code, which is, as in section XII, PRN 1 code. The isolation is then calculated between the autocorrelation value and the maximum of the cross-correlations between it and PRNs 2 to 9 are calculated. The process is repeated 1000 times, and the isolations are averaged.

Results are presented in Table 3. FDAF decreases the isolation only by a few tenths of dB, which should not significantly decrease the mean acquisition time performance. This result is tremendous, given that the mean acquisition time improvement is one of the main FDAF forwards, with tracking performance improvements. Once again, FDAF shows better performance than TB.

**Table 3: FDAF impact on PRN isolation degradation between PRN 1 and PRNs 2 to 9**

| **Isolation** | PRN 2 | PRN 3 | PRN 4 | PRN 5 |
|---|---|---|---|---|
| | 0.05 dB | 0.35 dB | 0.59 dB | 0.16 dB |
| | PRN 6 | PRN 7 | PRN 8 | PRN 9 |

| | | | | |
|---|---|---|---|---|
| | -0.04 dB | 0.27 dB | 0.46 | 0.51 |

## CONCLUSION

IMTs performances have been assessed from different angles. First, their capacity to reduce $C/N_0$ degradations due to pulsed interference has been shown. TB allows tracking GNSS signals with a degradation of 9.2 dB, while using FDAF this degradation is reduced to 3 dBs. These improvements allow better tracking accuracy, but also faster acquisition and lower data demodulation error rate. In addition, these results were obtained using a real AGC loop, which was supposed to decrease the techniques performance. The good robustness of the chosen AGC implementation to pulsed interference allows a degradation of the $C/N_0$ smaller than 0.5 dB, which is acceptable, given the large improvements previously quoted.

It also has been shown that FDAF was equivalent to a zero phase filter, thus not creating discontinuities in the tracked signal phase. This property has been verified through simulations, were code and carrier phase measurements observed standard deviations matched theoretical ones, whatever the used IMT.

Using TB, the PRN isolation is decreased by 2.5 dB, and only a few tenth of dB using FDAF. Thus FDAF is, once again, the best candidate for pulsed interference mitigation. Using TB, the false acquisition probability is highly increased, and so will be the mean acquisition time, whereas it will not be impacted using FDAF. The mean acquisition time is a critical parameter for civil aviation, so that the improvements brought by FDAF cannot be ignored.

## ACKNOWLEDGMENTS

This work has been funded by the ANASTASIA project. This project is financed through EC DG Research in the framework of FP6.

## REFERENCES

[Bastide, 2004], Bastide F.: *Analysis of the Feasibility and Interests of Galileo E5a/E5b and GPS L5 Signals for Use with Civil Aviation*, PhD. Thesis, 2004.

[Monnerat, 2003], Monnerat M., Erhard P., Lobert B.: *Performance Analysis of a GALILEO Receiver Regarding the Signal Structure, Multipath, and Interference Conditions*, ION GNSS 2003.

[Grabowsky, 2002], Grabowsky J., Hegarty C.: *Characterization of L5 Receiver Performance Using Digital Pulse Blanking*, Proceeding of The Institute of Navigation GPS Meeting, Portland, OR, September 2002.

[Van Dierendonck, 1996], Van Dierendonck A.J.: *"GPS receivers"*, *Global Positioning System: Theory and Application*, B.Parkinson and J.J Spilker, JR., Ed ., Washington, D.C.: AIAA, Inc., 1996.

[Raimondi, 2006], Raimondi M., Macabiau C., Bastide F., Julien O.: *Mitigating Pulsed Interference Using Frequency Domain Adaptive Filtering*, ION GNSS 2006.

[Betz, 2000], Betz J.W.: *Effect of Narrowband Interference on GPS Code Tracking Accuracy, Proceedings of the Institute of Navigation Technical Meeting*, Anaheim, CA, January 2000.